Accurate determination of bubble size and expansion ratio for polymer foaming with non-isothermal PBB model based on additional energy conservation

Yukai Ge, Zhiying Fang, Tao Liu*

Shanghai Key Laboratory of Multiphase Materials Chemical Engineering, East China University of Science and Technology, Shanghai 200237, P. R. China.

* Corresponding author: liutao@ecust.edu.cn (T. Liu)

Abstract: A non-isothermal pressure-balanced bubble-growth (PBB) model has been proposed based on mass, momentum and energy conservation, which additionally considered the decrease in the internal energy of gas due to the work done by gas expansion in bubble. The model could accurately predict the bubble size and expansion ratio for the melt foaming of four polymers for a wide range of cell densities from 1.5×10^{13} to 1.9×10^{15} cells/m^3. Furthermore, the simulation results indicate that the bubble shell resisted bubble growth and consumed significant energy, preventing the growth of some small nucleations. During the melt foaming process, the energy cost of the linear polymer had a long-term effect, which reduced the bubble size, while that of the long-chain branched polymer had a short-term effect, thereby increasing the expansion ratio. Finally, we defined the gas efficiency of the foaming agent to evaluate the economic feasibility of the foaming agent in a foaming process.

Keywords: Non-isothermal PBB model; Bubble growth simulation; Energy conservation; Bubble size distribution; Gas efficiency

1. Introduction

Polymer melt foaming is an important process owing to its scientific and industrial applicability.[1] The density and bubble size distribution (BSD) of polymer foams are critical to foam quality. Several events, such as nucleation, bubble growth, possible coalescence and rupture[2] and final solidification, occur during the foaming process and determine the final density and BSD of the foam.[3] The first nucleation is the initial state of a bubble from which the bubble grows. Nucleation strongly depends on process parameters such as pressure and temperature, especially nucleation agents,[4,5] indicating that nucleation is adjustable in some aspects. Some effective nucleation agents have been used to control cell density, such as nano-$CaCO_3$[6], nano-clay[7–9], nano-graphite[10] and multi-walled carbon nanotubes (MWCNTs)[10–13]. The nucleation and later bubble growth controlled the final density and BSD, which had considerable impact on the mechanical properties of the foam. For example, Bai et al.[14] found that the compressive strength and hardness of the prepared silicone rubber foams were improved as the cell diameter decreased from 4.97 to 1.12 μm. Kabir et al.[15] used a Zwick/Rowell machine to test the tensile and fracture behaviours of polyvinyl chloride (PVC) foam and rigid polyurethane foam, and found that the tensile strength and modulus were strongly dependent on the foam density.

Visual observation directly facilitates the understanding of the growth of bubbles through visual foam growth experiments[16]. Guo et al.[17] observed the foaming process

of polystyrene in a visualized autoclave and found that bubble growth was extremely sensitive to pressure drop. It only took 0.05 s to complete the bubble growth at an extremely high rate of pressure drop. Wong et al.[18] observed that the bubble growth behaviour changed with the macroscopic matrix deformation. As observed by Tammaro et al.[19], the main bubble growth process of a bulk sample could last for 20–30 s. Although these observations can help us observe the specific bubble growth process, the experimental phenomena could only provide a limited improvement in the understanding of the foaming mechanism.

Bubble growth determines the structure and properties of foams[1,20], thus being a crucial step for preparing polymer the foam with a uniform microcell structure. To deeply understand the mechanism of bubble growth, a few numerical models have been proposed.[1,21–27] The bubble growth model can be distinguished according to the region of a single bubble, that is, finite shell and infinite shell. Some scholars[24,26,28] studied diffusion-induced bubble growth in infinite mediums. Because the infinite shell provided an infinite amount of foaming agent, endless bubble growth could be observed. In the case of a finite bubble shell, the bubble stops growing after growing to a certain extent, which depends on the predetermined value of the shell volume. Li et al.[29] simulated the bubble growth of polypropylene (PP) with a finite shell, and their simulation showed that the bubble growth could stop and reach equilibrium. However, in their simulation, the final radius of a bubble was approximately 1250 times larger

than the initial value, which appeared extremely large compared to the actual situation. Feng et al.[1] attempted to predict the bubble size using the finite shell model and described the shell melt using the Oldroyd-B model. The fitting results were in good agreement with the experimental results, but a rapid pressure drop was not investigated, and the coverage was small. Ge et al.[20] proposed a pressure-balanced bubble-growth (PBB) model following the concept of finite volume. The model was unable to determine the final bubble radius effectively if the actual bubble density was used as the input.

Almost all the bubble growth models available assume that the bubble growth process is isothermal, and no in-situ measurement technology is available to challenge this assumption. The terminated bubble size considerably depends on its inner pressure[5,20,30–32], which is related to the gas temperature and inner energy. The bubble size calculation deviates from the real values if the gas temperature in the bubble is assumed to be unchanged. Thus, it is meaningful to consider the temperature change in the inner bubble[22,33,34]. Moreover, the bubble growth also determines the expansion ratio, and a correct bubble size calculation can result in an accurate theoretical expansion ratio. Therefore, an accurate bubble size calculation is of great significance, wherein the inner bubble temperature is one of the key factors.

In the present study, we proposed a non-isothermal PBB model from the viewpoint of mass, momentum, and energy conservation, which considered the

decrease in the internal energy of the gas owing to the work done performed by gas expansion. The model was used to predict the bubble size and expansion ratio for the melt foaming of four different polymers in a wide range of cell densities. The gas efficiency of the foaming agent was defined as Gas efficiency was defined as the changing rate of expansion ratio to the foaming pressure, providing a method to evaluate the economic feasibility of the foaming agent in the foaming process.

2. Experiments

2.1 Materials

The foaming behaviours of four types of materials were studied in this work. Pellets of low-density polyethylene (LDPE) (DFDA-1253NT) were supplied by Dow Chemical Co. Ltd., China. linear (L) structure polypropylene (PP) (T1903) was provided by Sinopec Maoming Petrochemical Co. Ltd., China. The long-chain branched (LCB-) PP (WB140) with a high melt strength was supplied by Borealis Co. Ltd. The LCB-PET was produced from a fibre-grade PET supplied by Xinshan Petrochemical Co. Ltd., China[20]. $CaCO_3$ nanospheres 40 nm in radius, tube-shaped MWCNTs 20 nm in length, lamellar nano graphite 40 nm in thickness, and nano clay 25 nm in thickness were supplied by XFNANO Chemical Co, Nanjing, China. CO_2 (purity: 99.9%, w/w %) and N_2 (purity: 99.9%, w/w %) were obtained from Air Production Co., Shanghai, China. All the chemical agents were used as received.

2.2 Molar mass characterization

The molar mass distribution was determined by size exclusion chromatography (Waters 1515). A linear polystyrene PS with a molar mass of 75 kg·mol^{-1} was used for calibration. The samples were pulverized and dissolved in hexafluoroisopropanol (HFLP) at a concentration of 4 g/L. All measurements were performed at 35 °C and a constant flow rate of 1.0 mL/min. **Table 1** lists the molecular information of the four polymers, and the details are given in the **Supporting Information**.

Table 1. Molecular structure parameters, CO_2 solubility, and interface parameters of the four polymers

Sample	M_w (kg/mol)	M_n (kg/mol)	M_w /M_n	LCB	γ (Pa/m)	H_a (g CO_2 /g melt/Pa)
LDPE[a]	107	25	11	very high	0.015	3.9×10^{-9}
LCB-PP[a]	609	80	8	high	0.013	5.6×10^{-9}
L-PP[a]	419	73	6	none	0.013	5.6×10^{-9}
LCB-PET[b]	65	28	2	very high	0.020	1.8×10^{-9}

[a]Molecular weight information was measured in this work.

[b]Molecular weight information was got from the reference 20.

2.3 Rheological characterization in shear and elongation

The linear viscoelasticity of the four polymers was measured using a Haake Mars III rheometer with a 35 mm plate fixture. Oscillation tests at a frequency range of 100–0.1 rad/s and at different temperatures were conducted in a nitrogen atmosphere.

The testing temperatures were 110, 130, and 160 °C for LDPE; 150, 180, and 200 °C for PP; and 265 °C for PET. The extensional viscosity of the four polymers was measured using a Sentmanat extensional rheometer (SER) fixture. Samples used in the measurements were cut into a shape of 20 mm length and 8 mm width.

The rheological behaviours of each polymer were also carefully modelled. In **Table 2**, three important parameters of each polymer are listed, including the zero shear viscosity and the two free factors that were used to describe strain hardening. In addition, the specific viscoelasticity analyses are presented in the **Supporting Information**. The molecular stress function (MSF) was used to describe the tensile behaviour of the melt. The details of the MSF model are available in the **Supporting Information**.

Table 2. Zero shear rate viscosity and non-linear parameters in MSF of the four polymers

Sample	$\eta_0^{\dot{\epsilon}}$(Pa·s)	B	f_{max}^2
LDPE	141000	1.8	80
LCB-PP	128000	1.6	100
Linear-PP	31959	1.0	4
LCB-PET	64970	2.4	120

2.4 Physical mixing of LDPE and different nucleation agents

The physical mixing of LDPE and 0.5 wt.% nucleation agents was conducted in a twin-screw extruder (Nanjing Giant SHJ-20). The screw length was 600 mm and the diameter was 20 mm. The speed of rotation was 350 rpm to obtain a strong shear for good blending. The temperature was set at 200 °C from the feeding to the die, and the material was fed at a rate of 10 kg/h. The nucleation agents added were $CaCO_3$ nanospheres, tube-shaped MWCNTs, lamellar nanographite, and nanoclay, respectively.

2.5 Batch foaming process at melt state

Batch foaming was conducted using a high-pressure vessel equipped with a pressure transducer. The high-pressure CO_2 used for foaming was provided by a TELIDE S-486-JN-60 pump. The temperature of the foaming system was controlled with an oil bath (± 0.5 °C). The samples used for foaming were first heated to 150 °C for LDPE, 180 °C for LCB-PP, and 265 °C for LCB-PET. Then, the samples were pressurised with CO_2 at a pressure range of 10–20 MPa at the same temperature held for 30 min. Subsequently, the system pressure was kept constant, and the processing temperature was reduced to the foaming temperature at which it was held for 60 min. The foaming temperatures were 110 °C for LDPE, 150 °C for LCB-PP, and 265 °C for LCB-PET. Thereafter, the pressure was rapidly released with a depressurization rate of approximately 100 MPa/s, leading to the formation of foamed cells. All

foaming experiments were conducted thrice under the same conditions.

2.6 Morphological analysis of polymer foams

Foaming samples were cooled in liquid nitrogen for 10 min and then fractured to achieve a cross-section. The cell morphology of the foam was observed using a scanning electron microscope (SEM) NOVE NanoSEM450 (FEI, USA). The information on cell size distribution was obtained through SEM photographs with the software Image-Pro Plus.[35]

3 Numerical simulation

3.1 Non-isothermal PBB model

The non-isothermal PBB model originated from the cell model[25], where the bubble shell was assumed to be a viscoelastic fluid having a finite volume. The bubble shell could hold a certain amount of foaming gas. The dissolved gas was transferred into the bubble and drove the bubble growth. In this process, three conservations including mass, momentum, and energy were involved, based on which, the non-isothermal PBB model was established. The isothermal assumption in the previous cell model required the total system including the bubble shell and inner gas to be isothermal. However, to achieve an accurate cell size calculation, a non-isothermal bubble growth model was necessary in which the change in gas temperature inside the bubble had to be considered. Meanwhile, the bubble shell

(solid phase) could be assumed to be isothermal for two reasons. First, in a polymer foaming bubble system, the mass of gas was more than one order of magnitude smaller than that of the polymer. For example, the solubility of CO_2 in LDPE was only 0.068 g gas/g LDPE[32]. Thus, the total inner energy of the gas was much smaller than that of the polymer, indicating that the temperature of the gas phase is more sensitive. Second, the polymer matrix deformation and friction also generated heat, which could offset the cooling caused by the gas. Moreover, the internal energy loss of the gas caused immediate temperature dropping of gas. When a gas expands and performs external work, the internal energy and temperature reduce instantly. Thus, it was reasonable to consider only the temperature change in the gas phase while the bubble shell remained isothermal. All the model assumptions are listed here:

(a) The bubble shell was isothermal, but the inner gas was non-isothermal.

(b) The bubble was spherical.[3]

(c) The polymer melt was incompressible.[3,24,25,27,29]

(d) The effect of plasticisation was ignored.[29]

(e) The effects of inertial forces and gravity could be neglected.[24]

(f) The bubble had no mass transfer with the environment, indicating that the bubble was a closed system.[29]

(g) The bubble growth rate followed the form of the Hencky strain, and the main

growth process was at a constant rate.[20]

(h) The inner pressure of the bubble depended on the amount and temperature of the gas inside the bubble, and the equilibrium vapor pressure of the polymer-gas solution was the driving force of mass transfer.[20]

3.2 Mass conservation

The mass of CO_2 in a closed bubble system follows the principle of mass conservation during bubble growth.

$$n_{CO_{2(\,system)}} = n_{CO_{2(\,inner\,bubble)}} + n_{CO_{2(\,dissolved)}} \tag{1}$$

$$n_{CO_{2(\,system)}} = H_a \cdot P_0 \cdot V_0 \tag{2}$$

$$n_{CO_{2(inner\,bubble)}} = \left(P¿¿¿ \cdot \left(\frac{4}{3}\pi R_i^3\right)\right)/\left(R\,T_¿\right)¿ \tag{3}$$

$$n_{CO_{2(dissolved)}} = c \cdot V_0 = H_a \cdot P_{eo} \cdot V_0 \tag{4}$$

$n_{CO_{2(\,system)}}$ represents the entire CO_2 in the bubble system, $n_{CO_{2(dissolved)}}$ the CO_2 dissolved in the bubble shell, and $n_{CO_{2(inner\,bubble)}}$ the CO_2 molar inner the bubble. R_i is the inner bubble radius, V_0 is the volume of the finite bubble shell, P_0 is the foaming pressure, and P_{in} is the bubble inner pressure. T_{in} is the bubble inner temperature. P_{eo} represents the

equilibrium vapor pressure of the CO_2/polymer solution, which can be described by Henry's law:

$$c = H_a \cdot P_{eo} \tag{5}$$

where H_a is the Henry′s coefficient of the CO_2/polymer solution, and c is the instantaneous concentration of CO_2. The final mass conservation equation is as follows:[5]

$$H_a \cdot P_0 \cdot V_0 = \frac{P_{¿}}{RT} \cdot \frac{4}{3}\pi R_i^3 + H_a \cdot P_{eo} \cdot V_0 \tag{6}$$

3.3 Momentum conservation

The principle of momentum conservation was satisfied during the bubble growth process. There were two differences compared to the traditional cell model[23–25,29]. First, the bubble growth rate was determined as a parameter of 5 s^{-1}.[20] In the rapid pressure dropping situation, the bubble growth time was short and its rate could be assumed to be a constant so that the corresponding bubble growth time was about 0.2 –0.3 s.[20] This time scale was close to the actual situation[17] in that, the bubble growth stage was less than 0.4 s under a rapid pressure relief rate. Second, the MSF model was used to calculate the elongational stress σ of the bubble shell. Despite the existence of small differences, both the form and meaning of the momentum equation were almost unchanged compared to the previous work.[23–25,29] The momentum equation of bubble growth is given by:

$$P_{¿} - P_e - \frac{2\gamma}{R_i} = 2\int_{R_i}^{R_{out}} \frac{\sigma_r + \eta^{¿}\dot{\gamma}_r}{r} dr \quad (7)$$

where P_e is the environmental pressure. The interface tension γ of the two phases lead to increased pressure inside the bubble. R_{out} is the outer radius of the bubble, where the shell thickness is included. $\eta^{¿}$ represents the melt viscosity, and $\dot{\gamma}$ represents the shear rate.

The LHS of the equation represents the total driven force, and the RHS is the resistance caused by the bubble shell. The growth resistance contains two different terms, that is, elongational stress and shear friction. Shear friction can be calculated by multiplying the viscosity and shear rate. The elongational stress σ_r of the bubble shell was calculated using the MSF[36–39]. Although other viscoelastic models were also available in stress calculations and were used in previous work, such as the upper-convected Maxwell[28] and Oldroyd-B models[1], the MSF possessed a few advantages—first, strain hardening was well described, which is a crucial property in foaming[5,40,41]. Second, a good connection between the molecular structure and the elongational properties was available. Härth et al.[42] used the MSF to model the elongational behaviour of LCB-PET and obtained a quantitative relationship between the branches and strain hardening. Ahirwal et al.[43]modeled the elongational behaviour of both PP and PE, and the MSF in both polymer systems showed accurate results. Therefore, the MSF model was selected for modelling the shell resistance of the matrix elongation.

3.4 Energy conservation

Bubble growth is a process of energy consumption, in which the gas expansion follows the first law of thermodynamics and can be regarded as a Carnot cycle[44]. When a high temperature gas is expanded outward, the gas temperature is decreased. The gas performs external work dring bubble growth, and this energy was consumed in matrix friction and stretching. Simultaneously, the inner energy of the bubble was supplemented because of the continuous evaporation of the foaming agent gas from the polymer matrix to the inner bubble. The foaming agent that was dissolved in the bubble shell was the energy source for bubble growth, and the stored energy decreased continuously because of the diffusion and evaporation. The bubble stopped growing when the system energy approached zero. The energy consumed in the bubble growth process can be regarded as the energy cost to change the polymer shape, that is, from the solid state to the foam form. The expanding energy in the bubble blowing process can be directly provided by the gas inside the bubble:

$$dW_{blow} = P_{¿} dV \tag{8}$$

$$P_{¿} dV = dU = nc_v dT_{¿} \tag{9}$$

$$c_v = \frac{i}{2} R_g \tag{10}$$

where d indicates a differential. W_{blow} is the work provided by the inner gas because of its expansion, and V is the bubble volume. The loss in gas inner energy U leads to a

decrease in the gas temperature T_{in}, and R_g is the gas constant. c_v is the specific heat capacity of the ideal gas, and for CO_2 with three atoms in one molecule, the parameter i is 6 according to the ideal gas theory.

A polymer/gas solution can provide high-pressure vapor, and, evidently, a certain amount of energy. The internal energy of the gas in the bubble was supplemented because of gas evaporation and diffusion from the bubble shell. During this period, the concentration of the gas/polymer solution as well as its energy, decreased. We quantified this energy and referred to it as the system energy E_{system}.

$$E_{system} = c H_a V_0 \tag{11}$$

H_a is the Henry's coefficient, c is the concentration, and V_0 is the shell volume. The system energy decreased with a reduction in the gas concentration:

$$dE_{system} = H_a V_0 dc \tag{12}$$

The mass transfer stops when the system energy becomes zero. Energy can be represented by pressure. The system energy E_{system} related to the vapor pressure P_{eo} is given by:

$$dE_{system} ¿ V_0 = P_{eo} \tag{13}$$

The blowing work (W_{blow}) leads to a temperature drop and pressure drop represented as P_w.

$$W_{blow} = \Delta n c_v T_¿ = \frac{c_v}{R_g} V \Delta P = \frac{c_v}{R_g} V P_w \quad (14)$$

P_w was ignored in traditional bubble growth models with an isothermal assumption. These models believed that the bubble stopped growing when the inner pressure equalled the vapor pressure i.e. $P_{eo} = P_{in}$. However, in the non-isothermal situation, the criterion for stopping the growth is $P_{eo} = P_{in} + P_w$.

3.5 Calculation procedure of bubble growth using non-isothermal PBB model

A flow chart of the non-isothermal PBB model is plotted for the calculation process specification. The initial conditions include the foaming temperature, pressure, and basic physical parameters, including Henry's constant and surface tension. The relaxation properties and strain hardening parameters in MSF are also required to describe the bubble shell deformation. Bubble growth simulation was conducted to obtain the values of P_{in}, W_{blow}, P_w, P_{eo}, and E_{system}. The expansion ratio and cell size were determined at end of the growth process. Veracious nucleation information was needed to determine the accurate cell size. Notably, the expansion ratio can be determined by using an assumed nucleation condition as well.

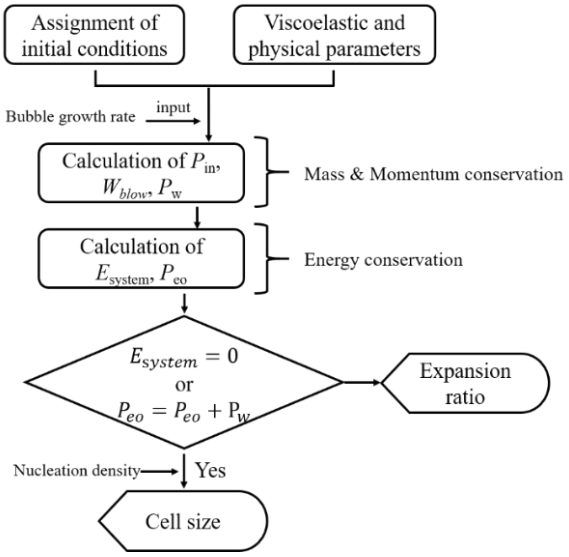

Figure 1. Computational flow chart of non-isothermal PBB model.

4. Results and discussion

4.1 Bubble growth simulation of LDPE foaming using non-isothermal PBB model

4.1.1 Bubble growth simulation of neat LDPE foaming

The batch foaming simulation and experiments using LDPE were conducted at 110 °C and 15 MPa CO_2. All the inputs of the simulation were determined by actual experiments. The cell density was determined to be 1.5×10^{13} cells/m^3 according to the SEM image shown in **Figure S4(a)** in the **Supporting Information**.

Figure 2 (a) shows the variations in system energy and blowing work during bubble growth. The simulation results were suitable for cell size calculation because the bubble growth stopped when the system energy reached zero. This occurred when the bubble grows to a radius of 70.0 μm. Accordingly, the theoretical bubble radius

was 70 μm, and the total blowing energy of one bubble was 2.6×10^{-7} (J). In **Figure 3**, the experimental results showed that the actual bubble diameter was 148 (μm), i.e., R_i = 74 μm, which agreed well with the theoretical calculation. If the bubble system comprised more energy, the growth could continue and obtain a higher expansion ratio. For example, Zhang et al.[32] used a mixture of CO_2 and i-C_4H_{10} as foaming agents. The cell diameter and expansion ratio increased with the amount of i-C_4H_{10}. It was because i-C_4H_{10} could store more gas and energy compared to CO_2 leading to a further bubble growth.

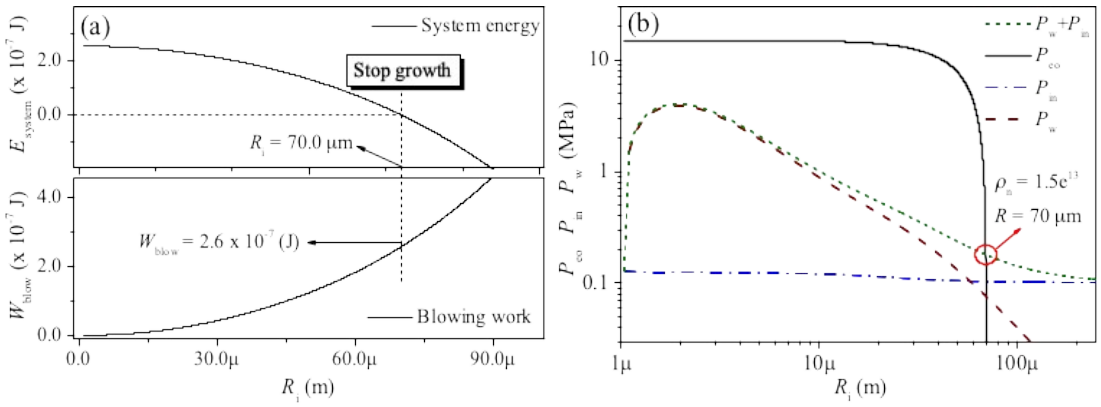

Figure 2. Simulation results of neat LDPE using non-isothermal PBB model. (a) Energy variations. (b) Pressure variations.

In **Figure 2(b)**, the simulation of bubble pressure can provide a detailed analysis of the bubble growth process. Three transfer behaviours, that is, energy, mass, and momentum, work together and determine the bubble growth behaviour. Three types of pressures are included—bubble inner pressure (P_{in}), gas phase equilibrium pressure (P_{eo}), and decreased pressure because of the gas expansion work (P_w). The P_{eo} curve is

mainly related to mass conservation, and P_{eo} declines after evaporation and the diffusion of CO_2 from the bubble shell. The P_{in} is controlled by momentum conservation, and energy conservation determines the P_w curve. A theoretical bubble radius can be found at the crossover point of the two curves, that is, the $P_w + P_{in}$ and P_{eo} curves. The radius calculated in the pressure form is the same as that calculated in the energy form.

As shown in **Figure 2(b)**, P_w increases rapidly at the initial bubble growth stage and then decreases slowly and continuously. The existence of the peak in the P_w curve at approximately 2 μm in radius has two reasons. First, the initial bubble was of micro dimensions, which meant that the bubble volume was small and the bubble shell was very thick, indicating that the resistance of bubble growth would be extremely large. Second, bubble growth consumed the internal energy of the gas, and the energy cost was related to resistance. The small amount of the internal energy of the gas was required to provide a large amount of energy at the initial bubble-growth stage, which led to a fast pressure drop corresponding to the peak in the P_w curve. Both the attenuation of the bubble shell and the increase in the gas amount weakened the influences of the expansion work. Thus, the P_w curve shows that the effects of gas inflation work and internal energy change were significant at the initial bubble growth stage, but would be mitigated later. Additionally, the gas temperature inside the bubble reveals the effects, as shown in **Figure S8** in the **Supporting Information**.

4.1.2 Bubble growth simulation of LDPE foaming under different nucleation conditions

Four different nucleation agents were used to change the density of the LDPE foams in the experiments. Foaming experiments were conducted under the same conditions as the neat LDPE, and the BSD of each foam was characterized according to the SEM images shown in **Figure S4** in the **Supporting Information**. **Figure 3** shows the morphology statistics of the different LDPE foams. The cell density varies more than one order of magnitude from 1.5×10^{13} cells/m^3 to 1.7×10^{14} cells/m^3 because of the use of different nucleation agents. Although the cell size changes significantly with cell density, the expansion ratio appears to be unaffected. The expansion ratios of the different LDPE foams vary around 24.

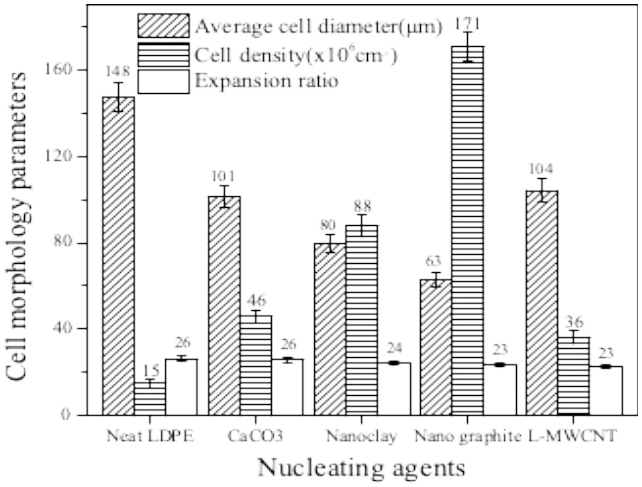

Figure 3. Morphology statistics of LDPE foams with different nucleation agents.

The cell density was updated in the simulation according to the SEM images.

The theoretical bubble growth processes were calculated, and the results are plotted in **Figure 4**. In addition to predicting the bubble size, two more meaningful results can be obtained by bubble growth simulation. First, according to the calculated bubble radius, the expansion ratio calculation is also available. The calculation results are consistent with the foaming experiments for both the average bubble size and expansion ratio, as shown in **Figure 5**. If the energy conservation is not considered, that is, in the isothermal situation, the calculated radius and expansion ratio will be much larger than the actual values. The calculated results, without considering energy conservation, contained significant errors in the expansion ratio up to approximately 58 %. However, the accuracy in both the bubble size and expansion ratio predictions was greatly improved by considering energy conservation. It was proven that the bubble growth is a non-isothermal process, and the energy cost of growth should be considered. Second, a high peak in the P_w curve appears at low nucleation density, indicating a considerable resistance in bubble growth. The nucleation density not only affects the potential cell number but also corresponds to the bubble growing resistance, which was not found in previous bubble growth simulations because the energy conservation was not considered. Correspondingly, a large nucleation size favours bubble growth and increases the final cell density. Accordingly, the ideal nucleation agents should satisfy two requirements, that is, providing a large number of nucleation points and a large nucleation size. Some early experimental phenomena could be explained by the simulation results. Chen et al.[45] found that the nucleation

agent, MWCNTs, with a small size had low nucleation efficiency at the low foaming pressure, but the density was improved after increasing the foaming pressure. Meanwhile, the large size of MWCNTs had a high nucleation efficiency at all foaming pressures. According to the simulation, a significant peak in the P_w curve appears if the nucleation size is small, indicating that it is challenging for the nucleation point to grow. In addition, the effects of P_w decrease after increasing the foaming pressure (related to P_{eo}) as the entire driven force is P_{eo} - P_w. Therefore, in the experiments conducted by Chen et al.[45], the high growth resistance, instead of fewer nucleation points, may be attributable for the low cell density when small MWCNTs were used.

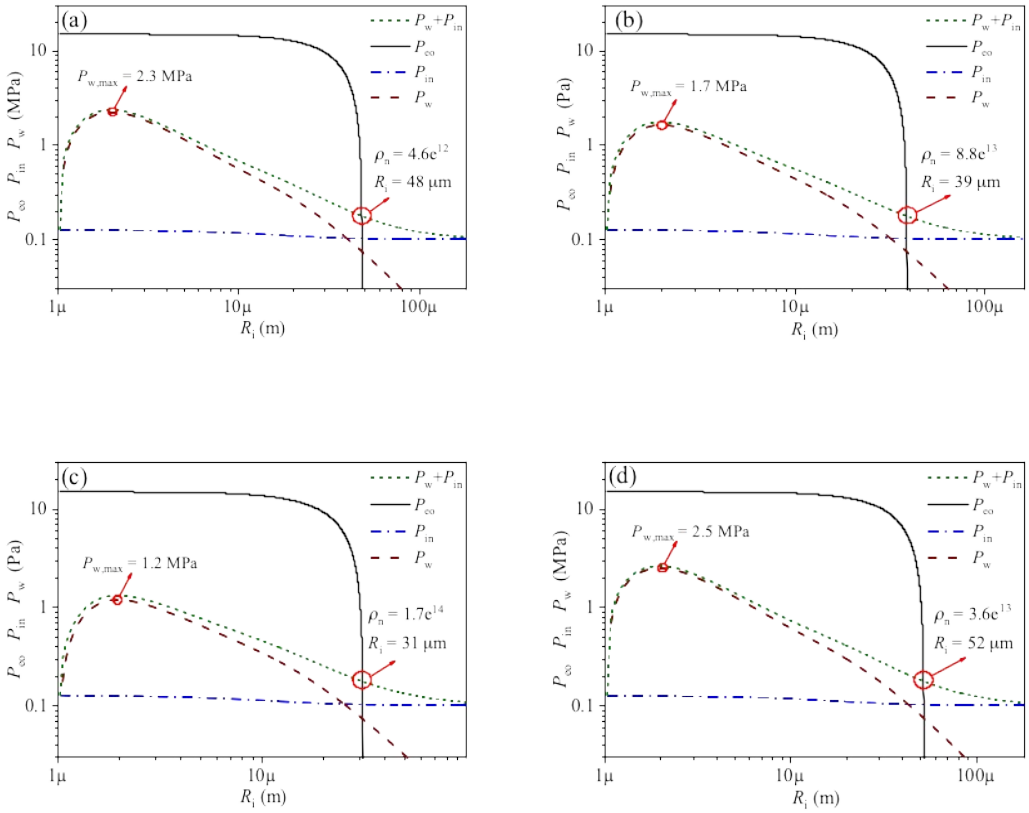

Figure 4. Bubble growth simulation for LDPE samples with nucleation agents. (a) $CaCO_3$/LDPE, (b) Nano-Clay/LDPE, (c) Nano-graphite/LDPE and (d) MWCNTs/LDPE.

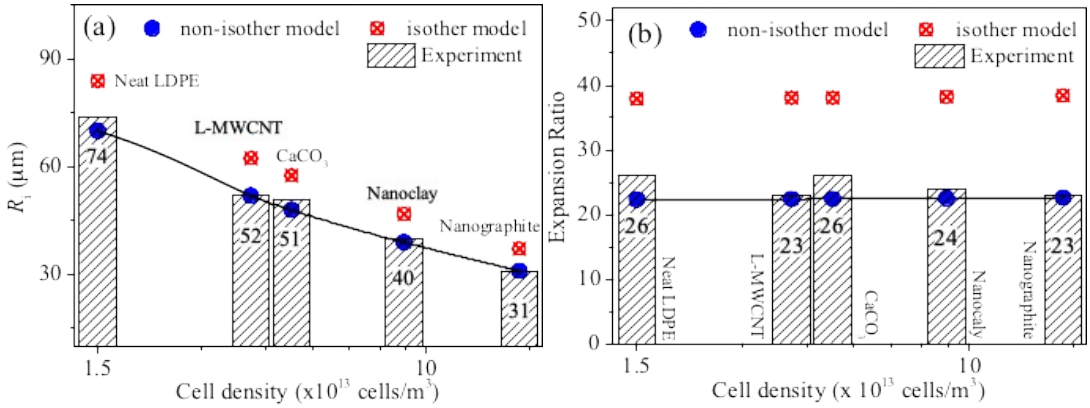

Figure 5. Comparison of foaming results and simulations with isothermal and non-isothermal models. (a) bubble radius, (b) expansion ratio. The lines only indicated the trend.

4.2 Bubble growth simulations of L-PP, LCB-PP, and LCB-PET foaming using non-isothermal PBB model

To explore the validity of the non-isothermal PBB model, bubble growth simulations for foaming of three different polymers— L-PP, LCB-PP, and LCB-PET — were also performed. Furthermore, foaming experiments were conducted, and the micromorphology of each foam was carefully analysed. The cell sizes were measured according to the SEM images shown in **Figure S5** of the **Supporting Information**. It was found that the BSD met a nearly normal distribution, as shown in **Figure S6** in the **Supporting Information**. Bubble growth simulations were conducted, in which all the inputs were equal to the exact conditions for the foaming experiments. The results, including the predicted bubble radius R_p, the exact cell size R_i, expansion ratio, and cell density ρ_n are listed in **Table 3**.

Table 3. Foaming conditions, morphology statistics of foams, and the model calculated results

Sample	T (°C)	P (MPa)	ρ_n[a] (cells/m^3)	R_i[a] (μm)	R_p[b] (μm)	Expansion Ratio[a&b]	Gas efficiency[b] (MPa^{-1})
LDPE	110	15	1.5×10^{13}	71	70	26 & 22	1.8
LCB-PP	150	15	1.0×10^{14}	47	47	40 & 45	3.5
L-PP	150	12	1.9×10^{14}	30	31	26 & 26	2.0^{1st}; 11^{2st}
LCB-PET	265	18	1.7×10^{15}	17	17	32 & 33	2.1

[a]Results obtained from experiments.

[b]Results obtained from simulations.

The termination of bubble growth can be easily determined when the system energy becomes zero, as shown in **Figures 6(a-1), (b-1),** and **(c-1)**. The blowing energy W_{blow} of each bubble is obtained. As shown in **Figure 6(c-1)**, LCB-PET has the lowest system energy and its blowing work is only 2.2×10^{-9} J/cell, which is one magnitude smaller than that of L-PP and LCB-PP, as shown in **Figures 6(a-1) and (b-1)**. The energy of LCB-PET is limited by the solubility of CO_2 in PET. As shown in **Table 1**, it has the lowest Henry's coefficient. Therefore, more system energy was required to obtain PET foam with a larger expansion ratio. The second reason for the low W_{blow} was that the cell density of PET was extremely high, and the bubble size was small.

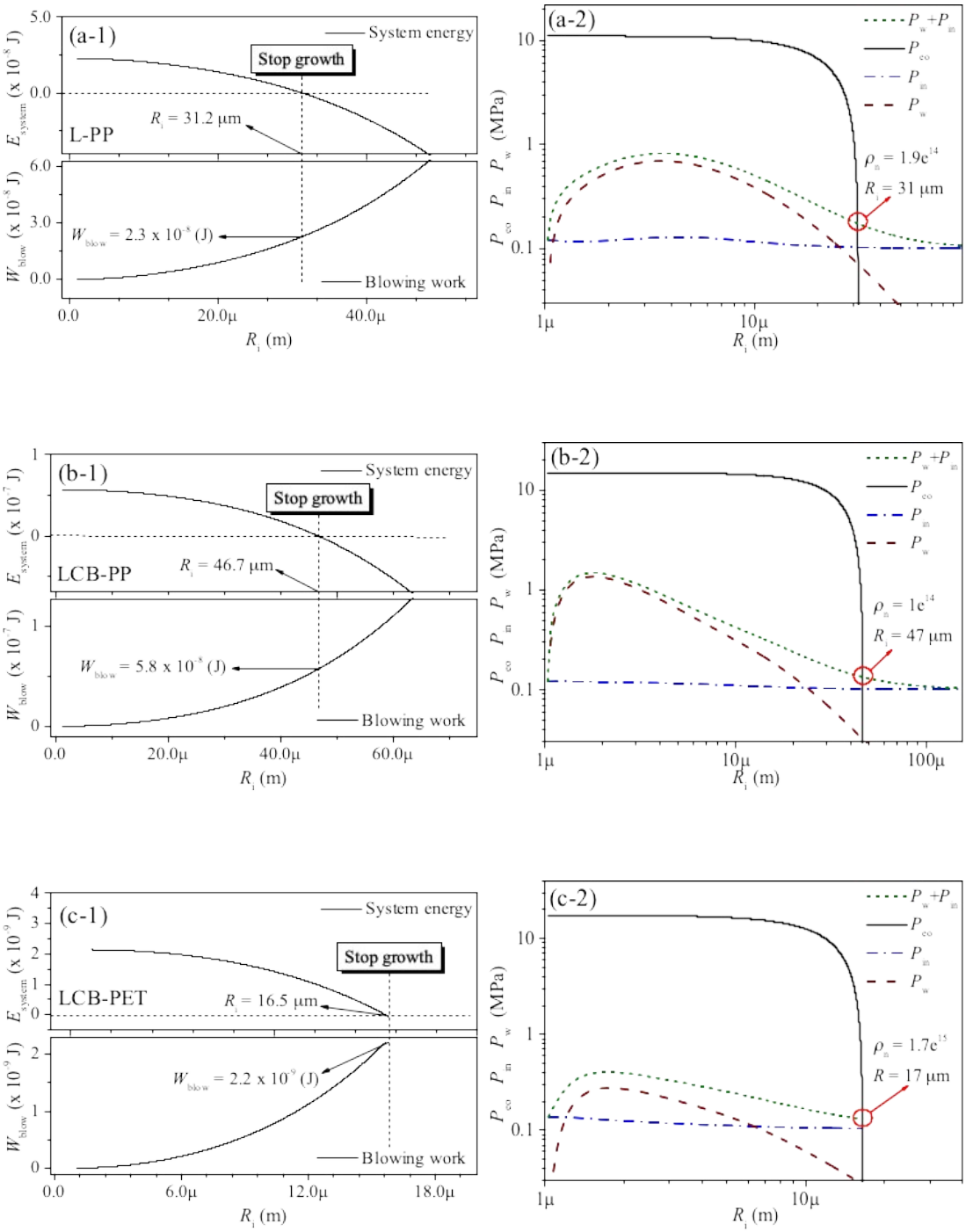

Figure 6. Simulations of polymer foaming using non-isothermal PBB model in energy form: (a-1) L-PP, (b-1) LCB-PP, (c-1) LCB-PET; and in pressure form: (a-2) L-PP, (b-2) LCB-PP, (c-2) LCB-PET.

The P_w curve has different shapes for the three polymers, which affects the

bubble growth behaviours. P_w was related to the energy loss owing to the growth resistance. For LCB-PP and LCB-PET, the corresponding P_w curves decrease rapidly, indicating that bubble growth faced a weak resistance. L-PP shows a near-elliptic P_w curve, which means that the inner energy cost affects bubble growth for a long period. The difference in the P_w curve is related to the polymer chain structure because linear and LCB structures have different elongational behaviours, as shown in **Figure S3** in the **Supporting Information**. The L-PP is more viscous and has a relatively flat elongational viscosity, while the LCB-PP has a low viscosity at the initial bubble growth stage and shows a significant increase in viscosity after stretching. Low initial viscosity indicates a weak resistance at the beginning of bubble growth. The subsequent increase in the elongational viscosity is beneficial to the foaming stability when the bubble wall becomes thin and weak after bubble growth. Therefore, a relatively low initial viscosity and a significant viscosity increase are the ideal rheological properties for the foaming process. Therefore, the LCB structure is more suitable for foaming applications than linear structure in both process stability and obtaining a high expansion ratio.

4.3 Gas efficiency in melt foaming of four polymers

In the foam industry, it is usually desirable to produce foams with a high expansion ratio under the lowest foaming pressure, so as to achieve profit and safety. However, the relationship between the expansion ratio and foaming pressure is often

unknown. To achieve an overall understanding of this relationship, gas efficiency (CO_2 in this work) was proposed in this work. Gas efficiency was defined as the changing rate of expansion ratio to the foaming pressure.

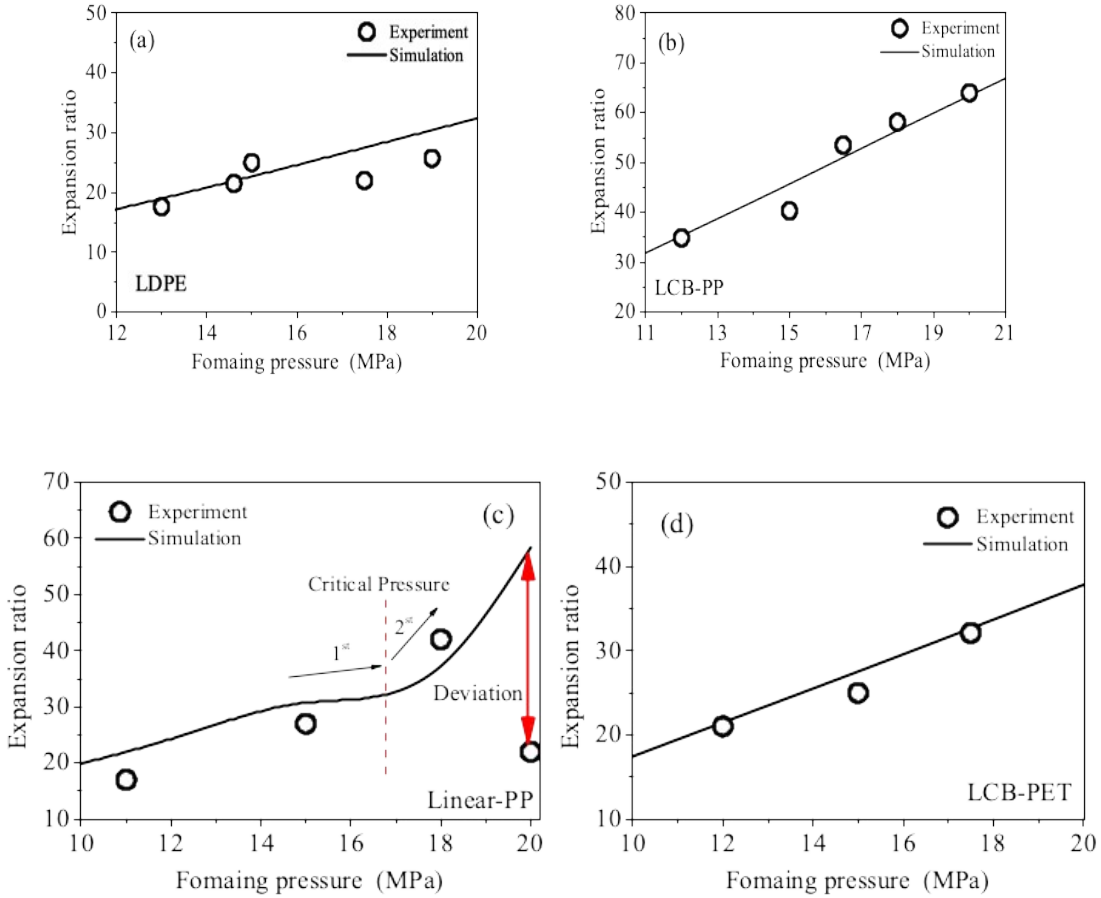

Figure 7. Determination of expansion ratio at different foaming pressures in both experiments and simulations. (a) LDPE, (b) LCB-PP, (c) L-PP, (d) LCB-PET.

Both the simulations and experiments were conducted in a pressure range of 11 to 20 MPa. In the simulations, only the expansion ratio was focused on, while the inputs of nucleation density, an ordinary value of 1×10^{13} cells/m^3, was assumed for all the samples. The simulated expansion ratios as a function of foaming pressure are

plotted in **Figure 7**. The results of the experiment and simulation show good agreement, which proves that the non-isothermal PBB model is an effective method for analysing the expansion ratio. It should be noted that the prediction at extreme high foaming pressures, such as above 20 MPa, contains errors because of plasticization[4,46].

The curve of the expansion ratio shows an almost linear shape for all the LCB-polymers, that is, LDPE, LCB-PP, and LCB-PET, as shown in **Figure 7(a)**, **(b)**, and **(c)**, indicating that their gas efficiencies are constant. However, the gas efficiencies of the three polymers are different: 1.8, 3.5, and 2.1 for LDPE, LCB-PP, and LCB-PET, respectively. The expansion ratio of LDPE is relatively insensitive to the foaming pressure, indicating that it is not an economical to obtain a high expansion PE foam using high-pressure CO_2. The gas efficiency of LCB-PET is similar to that of LDPE, which means that CO_2 alone is insufficient to achieve a satisfactory expansion ratio. However, the reason for the low gas efficiencies is different for the two polymers. For LDPE, the main reason is the high melt viscosity, which consumes a large amount of energy. For LCB-PET, it has a low solubility of CO_2, leading to a low expansion ratio. The gas efficiency of LCB-PP is favourable, which means that the use of CO_2 in PP foaming is economical, and 20 MPa CO_2 is sufficient to produce PP foam with a high expansion ratio of 65.

The L-PP shows a considerably different outcome, and its expansion ratio curve

exhibits nonlinearity. By increasing the foaming pressure to approximately 17 MPa, an accelerated increase in the expansion ratio is observed. The gas efficiency at low foaming pressure is small and approximately 2.0 (MPa^{-1}), but increases to 11 (MPa^{-1}) at high foaming pressure. The appearance of the second stage, in which the gas efficiency increases, is caused by the linear structure of L-PP. The initial viscosity of L-PP is high, which is the reason for the low gas efficiency at the first stage. Compared with the LCB-polymers, the L-PP has a low elongational viscosity after stretching because of the lack of strain hardening, indicating low growth resistance at the late bubble growth stage. A deviation between the experiments and simulations appears at a foaming pressure of 20 MPa for the L-PP system, as shown in **Figure 7(c)**. The SEM images shown in **Figure S7** in the **Supporting Information** indicate that the L-PP foam produced at 20 MPa has cell wall rupture behaviour, which led to an open-cell structure. This morphology did not satisfy the model assumption that the bubble system was a sealed sphere. The gas and corresponding energy leaked at the rupture point, leading to a low expansion and an open-cell structure. This phenomenon also indicated that the bubble shell might be broken under an extremely high foaming pressure.

Conclusion

A non-isothermal PBB model was proposed from the viewpoint of mass, momentum, and energy conservation, which additionally considered the decrease in

gas internal energy owing to the work performed by gas expansion in the bubble. Accurate predictions of bubble size and expansion ratio for the polymer foaming process were made with the model calculation. The model correction was verified in four kinds of polymers and in a wide range of cell densities from 1.5×10^{13} cells/m^3 to 1.9×10^{15} cells/m^3. The simulation results indicated that some nucleation points were difficult to grow because of shell resistance, leading to a significant energy cost. Furthermore, the effects of gas expansion work on bubble growth were different for linear and LCB polymers; a relatively prolonged decrease in the inner pressure appeared for the linear situation. Finally, the gas efficiency of foaming was theoretically calculated. The gas efficiency of CO_2 for PP foaming was satisfactory, while for PE and PET, single CO_2 demonstrated a low gas efficiency.

Acknowledgements

This work was supported by the National Key Research and Development Program of China (2016YFB0302200) and the Fundamental Research Funds for the Central Universities (22221818014).

Reference

1. Feng JJ, Bertelo CA. Prediction of bubble growth and size distribution in polymer foaming based on a new heterogeneous nucleation model. *J Rheol*. 2004;48(2):439-462. doi:10.1122/1.1645518

2. Ge YK, Liu T. Numerical simulation on bubble wall shape evolution and uniformity in poly(ethylene terephthalate) foaming process. *Chem Eng Sci*. 2020; (xxxx):116213. doi:10.1016/j.ces.2020.116213

3. Amon M, Denson CD. A study of the dynamics of foam growth: Analysis of the growth of closely spaced spherical bubbles. *Polym Eng Sci*. 1984;24(13):1026-1034. doi:10.1002/pen.760241306

4. Wan C, Lu Y, Liu T, Zhao L, Yuan W. Foaming of low density polyethylene with carbon dioxide based on its in situ crystallization behavior characterized by high-pressure rheometer. *Ind Eng Chem Res*. 2017;56(38):10702-10710. doi:10.1021/acs.iecr.7b02842

5. Ge YK, Yao S, Xu ML, Gao L, Fang ZY, Zhao L, Liu T. Improvement of poly(ethylene terephthalate) melt-foamability by long-chain branching with the combination of pyromellitic dianhydride and triglycidyl isocyanurate. *Ind Eng Chem Res*. 2019;58(9):3666-3678. doi:10.1021/acs.iecr.8b04157

6. Xi Z, Chen J, Liu T, Zhao L, Turng LS. Experiment and simulation of foaming injection molding of polypropylene/nano-calcium carbonate composites by supercritical carbon dioxide. *Chinese J Chem Eng*. 2016;24(1):180-189. doi:10.1016/j.cjche.2015.11.016

7. Zhai W, Kuboki T, Wang L, Park CB, Lee EK, Naguib HE. Cell structure evolution

and the crystallization behavior of polypropylene/clay nanocomposites foams blown in continuous extrusion. *Ind Eng Chem Res*. 2010;49(20):9834-9845. doi:10.1021/ie101225f

8. Taki K, Yanagimoto T, Funami E, Okamoto M, Ohshima M. Visual observation of CO_2 foaming of polypropylene-clay nanocomposites. *Polym Eng Sci*. 2004;44(6):1004-1011. doi:10.1002/pen.20093

9. Zeng C, Han X, Lee LJ, Koelling KW, Tomasko DL. Polymer-Clay Nanocomposite Foams Prepared Using Carbon Dioxide. *Adv Mater*. 2003;15(20):1743-1747. doi:10.1002/adma.200305065

10. Baseghi S, Garmabi H, Gavgani JN, Adelnia H. Lightweight high-density polyethylene/carbonaceous nanosheets microcellular foams with improved electrical conductivity and mechanical properties. *J Mater Sci*. 2015;50(14):4994-5004. doi:10.1007/s10853-015-9048-3

11. Jiang R, Chen Y, Yao S, Liu T, Xu ZM, Park CB, Zhao L. Preparation and characterization of high melt strength thermoplastic polyester elastomer with different topological structure using a two-step functional group reaction. *Polymer*. 2019;179:121628. doi:10.1016/j.polymer.2019.121628

12. Yeh JM, Chang KC, Peng CW, Chand B, Chiou SC, Huang HH, Lin CY, Yang JC. Preparation and insulation property studies of thermoplastic PMMA-silica

nanocomposite foams. *Polym Compos*. 2009;30(6):715-722. doi:10.1002/pc.20601

13. Yan DX, Dai K, Xiang ZD, Li ZM, Ji X, Zhang WQ. Electrical conductivity and major mechanical and thermal properties of carbon nanotube-filled polyurethane foams. *J Appl Polym Sci*. 2011;120(5):3014-3019. doi:10.1002/app.33437

14. Bai J, Liao X, Huang E, Luo Y, Yang Q, Li G. Control of the cell structure of microcellular silicone rubber/nanographite foam for enhanced mechanical performance. *Mater Des*. 2017;133:288-298. doi:10.1016/j.matdes.2017.07.064

15. Kabir ME, Saha MC, Jeelani S. Tensile and fracture behavior of polymer foams. *Mater Sci Eng A*. 2006;429(1-2):225-235. doi:10.1016/j.msea.2006.05.133

16. Wong A, Guo Y, Parka CB. Fundamental mechanisms of cell nucleation in polypropylene foaming with supercritical carbon dioxide - Effects of extensional stresses and crystals. *J Supercrit Fluids*. 2013;79:142-151. doi:10.1016/j.supflu.2013.02.013

17. Guo Q, Wang J, Park CB, Ohshima M. A microcellular foaming simulation system with a high pressure-drop rate. *Ind Eng Chem Res*. 2006;45(18):6153-6161. doi:10.1021/ie060105w

18. Wong A, Park CB. The effects of extensional stresses on the foamability of polystyrene-talc composites blown with carbon dioxide. *Chem Eng Sci*. 2012;75:49-62. doi:10.1016/j.ces.2012.02.040

19. Tammaro D, Contaldi V, Carbone MGP, Di Maio E, Iannace S. A novel lab-scale batch foaming equipment: The mini-batch. *J Cell Plast*. 2016;52(5):533-543. doi:10.1177/0021955X15584654

20. Ge YK, Lu JW, Liu T. Analysis of bubble coalescence and determination of the bubble radius for long−chain branched poly(ethylene terephthalate) melt foaming with a pressure balanced bubble−growth model. *AIChE J*. 2020;66(4):1-13. doi:10.1002/aic.16862

21. Aloku GO, Yuan XF. Numerical simulation of polymer foaming process in extrusion flow. *Chem Eng Sci*. 2010;65:3749-3761. doi:10.1016/j.ces.2010.03.022

22. Sun Y, Ueda Y, Suganaga H, Haruki M, Kihara SI, Takishima S. Experimental and simulation study of the physical foaming process using high-pressure CO_2. *J Supercrit Fluids*. 2016;107:733-745. doi:10.1016/j.supflu.2015.08.001

23. Goel SK, Beckman EJ. Nucleation and growth in microcellular materials: supercritical CO_2 as foaming agent. *AIChE J*. 1995;41(2):357-367.

24. Chen Y, Wan C, Liu T, et al. Evaluation of LLDPE/LDPE blend foamability by in situ rheological measurements and bubble growth simulations. *Chem Eng Sci*. 2018;192:488-498. doi:10.1016/j.ces.2018.07.051

25. Leung SN, Park CB, Xu D, Li H, Fenton RG. Computer simulation of bubble-growth phenomena in foaming. *Ind Eng Chem Res*. 2006;45(23):7823-7831.

doi:10.1021/ie060295a

26. Venerus DC. Diffusion-induced bubble growth and collapse in yield stress fluids. *J Nonnewton Fluid Mech*. 2015;215:53-59. doi:10.1016/j.jnnfm.2014.11.001

27. Venerus DC. Diffusion-induced bubble growth in viscous liquids of finite and infinite extent. *Polym Eng Sci*. 2001;41(8):1390-1398. doi:10.1002/pen.10839

28. Venerus DC, Yala N, Bernstein B. Analysis of diffusion-induced bubble growth in viscoelastic liquids. *J Nonnewton Fluid Mech*. 1998;75(1):55-75. doi:10.1016/S0377-0257(97)00076-1

29. Li Y, Yao Z, Chen Z hua, Cao K, Qiu SL, Zhu FJ, Zeng CC, Huang ZM. Numerical simulation of polypropylene foaming process assisted by carbon dioxide: Bubble growth dynamics and stability. *Chem Eng Sci*. 2011;66(16):3656-3665. doi:10.1016/j.ces.2011.04.035

30. Yue P, Feng JJ, Bertelo CA, Hu HH. An arbitrary lagrangian-eulerian method for simulating bubble growth in polymer foaming. *J Comput Phys*. 2007;226:2229:2249. doi:10.1016/j.jcp.2007.07.007

31. Kharbas HA, Ellingham T, Manitiu M, Scholz G, Turng LS. Effect of a cross-linking agent on the foamability of microcellular injection molded thermoplastic polyurethane. *J Cell Plast*. 2017;53(4):407-423. doi:10.1177/0021955X16652109

32. Zhang H, Fang Z, Liu T, Li B, Li H, Cao ZH, Jin G, Zhao L. Dimensional

stability of LDPE foams with CO_2 + i-C4H10 mixtures as blowing agent: experimental and numerical simulation. *Ind Eng Chem Res*. 2019;58(29):13154-13162. doi:10.1021/acs.iecr.9b02501

33. Taki K. Experimental and numerical studies on the effects of pressure release rate on number density of bubbles and bubble growth in a polymeric foaming process. *Chem Eng Sci*. 2008;63(14):3643-3653. doi:10.1016/j.ces.2008.04.037

34. Leung SN, Li H, Park CB. Impact of approximating the initial bubble pressure on cell nucleation in polymeric foaming processes. *J Appl Polym Sci*. 2007;104(2):902-908. doi:10.1002/app.25728

35. Song C, Li S, Zhang J, Xi Z, Lu E, Zhao L, Cen L. Controllable fabrication of porous PLGA/PCL bilayer membrane for GTR using supercritical carbon dioxide foaming. *Appl Surf Sci*. 2019;472:82-92. doi:10.1016/j.apsusc.2018.04.059

36. Narimissa E, Rolón-Garrido VH, Wagner MH. A hierarchical multi-mode MSF model for long-chain branched polymer melts part I: elongational flow. *Rheol Acta*. 2015;54(9-10):779-791. doi:10.1007/s00397-015-0879-2

37. Narimissa E, Rolón-Garrido VH, Wagner MH. A hierarchical multi-mode MSF model for long-chain branched polymer melts part II: multiaxial extensional flows. *Rheol Acta*. 2016;55(4):327-333. doi:10.1007/s00397-016-0922-y

38. Rolón-Garrido VH. The molecular stress function (MSF) model in rheology.

Rheol Acta. 2014;53:663-700. doi:10.1007/s00397-014-0787-x

39. Aho J, Rolón-Garrido VH, Syrjälä S, Wagner MH. Measurement technique and data analysis of extensional viscosity for polymer melts by Sentmanat extensional rheometer (SER). *Rheol Acta*. 2010;49(4):359-370. doi:10.1007/s00397-010-0439-8

40. Fan C, Wan C, Gao F, et al. Extrusion foaming of poly(ethylene terephthalate) with carbon dioxide based on rheology analysis. *J Cell Plast*. 2016;52(3):277-298. doi:10.1177/0021955X14566085

41. Yang Z, Xin C, Mughal W, Li X, He Y. High-melt-elasticity poly(ethylene terephthalate) produced by reactive extrusion with a multi-functional epoxide for foaming. *J Appl Polym Sci*. 2018;135(8):45805. doi:10.1002/app.45805

42. Härth M, Kaschta J, Schubert DW. Shear and elongational flow properties of long-chain branched poly(ethylene terephthalates) and correlations to their molecular structure. *Macromolecules*. 2014;47(13):4471-4478. doi:10.1021/ma5002657

43. Ahirwal D, Filipe S, Neuhaus I, Busch M, Schlatter G, Wilhelm M. Large amplitude oscillatory shear and uniaxial extensional rheology of blends from linear and long-chain branched polyethylene and polypropylene. *J Rheol*. 2014;58(3):635-658. doi:10.1122/1.4867555

44. Andresen B, Berry RS, Nitzan A, Salamon P. Thermodynamics in finite time. I. The step-Carnot cycle. *Phys Rev A*. 1977;15(5):2086-2093.

doi:10.1103/PhysRevA.15.2086

45. Chen L, Ozisik R, Schadler LS. The influence of carbon nanotube aspect ratio on the foam morphology of MWNT/PMMA nanocomposite foams. *Polymer*. 2010;51(11):2368-2375. doi:10.1016/j.polymer.2010.03.042

46. Tsivintzelis I, Angelopoulou AG, Panayiotou C. Foaming of polymers with supercritical CO2: An experimental and theoretical study. *Polymer*. 2007;48(20):5928-5939. doi:10.1016/j.polymer.2007.08.004